24th COBEM - 2017

24th ABCM International Congress of Mechanical Engineering
December 3-8, 2017, Curitiba, PR, Brazil

COBEM-2017-1154
THE INFLUENCE OF SPEED AND SLOPE ANGLE ON WHEELCHAIR PROPULSION PATTERNS: AN OPTIMAL CONTROL STUDY

Vinicius I. Cuerva
Marko Ackermann
Fabrizio Leonardi
FEI University, Department of Mechanical Engineering
Av. Humberto de Alencar Castelo Branco, 3972, CEP: 09850-901 - São Bernardo do Campo, Brazil
vini.shimoto@gmail.com.br, mackermann@fei.edu.br, fabrizio@fei.edu.br

Abstract. *The wheelchair is one of the most used assistive devices for people with locomotion disability. However, manual wheelchair propulsion is inefficient and can impose excessive loads on the upper limbs, increasing the risk of injury. The hand trajectory during the propulsion cycle may be a factor affecting efficiency and upper extremity loads. Previous investigations have assessed the strategies adopted by wheelchair users in different situations, but all of them were based on experimental analyses, which limited the number of investigated scenarios. Moreover, generally the experiments are performed on treadmills or rollers, which can artificially affect the adopted strategy. In this study, a multibody model of the wheelchair user system is used in combination with an optimal control formulation to generate predictive simulations of steady-state wheelchair propulsion and investigate the influence of different velocities and slope angles on hand trajectory. The results are compared to experimental data from the literature and provide insights on the mechanics of wheelchair propulsion and its influence on hand motion patterns.*

Keywords: *wheelchair propulsion, optimal control, hand motion patterns, propulsion techniques.*

1. INTRODUCTION

Wheelchairs are among the most used means of assistance for people with lower limb disabilities. In spite of the widespread usage worldwide, the wheelchair locomotion is associated with upper limb injuries and inefficiency, among others, due to the relative small muscle mass of the upper limbs compared to the lower limbs and the unfavorable upper extremity trajectory during the propulsion cycle with traditional hand-rim wheelchairs (van der Woude *et al.*, 2001).

The wheelchair propulsion cycle is composed by two phases: the propulsion phase, where the hands are in contact with the pushrim, and the recovery phase, where the hands do not contact the pushrim and the upper extremities are repositioned in preparation to the next propulsion phase. The adopted propulsion technique may influence the efficiency of locomotion, increase the propulsion frequency and cause the appearance of resisting contact forces on the pushrims (Vegter *et al.*, 2014).

The hand patterns during wheelchair propulsion are commonly classified into four different categories: arcing over the handrim (AR), single loop above the handrim (SL), semi-circular pattern below the handrim (SC) and double-loop pattern (DL), where the hands pass first above the handrim in the recovery phase and then below it (Slowik *et al.*, 2015), refer to Fig. 1.

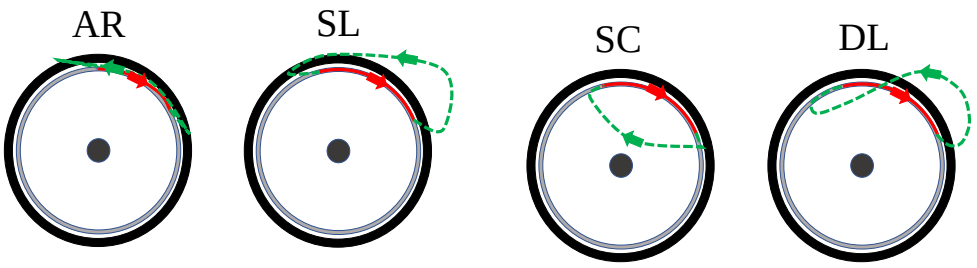

Figure 1. Possible hand patterns in manual wheelchar propulsion: arcing over the handrim (AR), single-loop above the handrim (SL), semi-circular below the handrim (SC) and dual loop above and below the handrim (DL).

Some variables related to the upper extremity demand in the propulsion cycle of a wheelchair such as push frequency,

peak force and contact angle are not independent between each other. The literature shows that minimizing those variables separately proved to be less effective in reducing the muscle demand than searching for a balance (Rankin *et al.*, 2012).

On ramps, the literature reports the use of hand motion patterns closer or above the pushrim, mainly to avoid the return of the wheelchair during the recovery phase (Richter *et al.*, 2007). In relation to the velocity, most studies report a transition from patterns under the pushrim at low velocities to patterns above the pushrim as velocity increases (Slowik *et al.*, 2015). However, at least one study indicates that this transition is more subtle than reported elsewhere (Boninger *et al.*, 2002), and the mechanical rational underlying the occurrence of this transition is not well understood.

In this context, the main objective of this study was to investigate the influence of speed and slope angle on the hand pattern during wheelchair propulsion using a simplified multibody system model, combined with an optimal control formulation. This framework may provide a better insight into the mechanics underlying pattern selection and could help instruct new wheelchair users about the better ways to propel a wheelchair.

2. METHODS

The model of the wheelchair and user system was formulated as a planar multibody system composed of 4 rigid bodies (arms, forearms, body+wheelchair, and wheels) connected by ideal hinge joint representing the upper limb articulations and actuated by elbow and shoulder joint moments (Fig. 2). The shoulder joint was assumed fixed to the wheelchair and no slip between the wheels and the floor was allowed. Bilateral symmetry was assumed, which is usual between wheelchair users (Goosey-Tolfrey and Kirk, 2003) and is a reasonable condition for the wheelchair propulsion cycle (Soltau *et al.*, 2015).

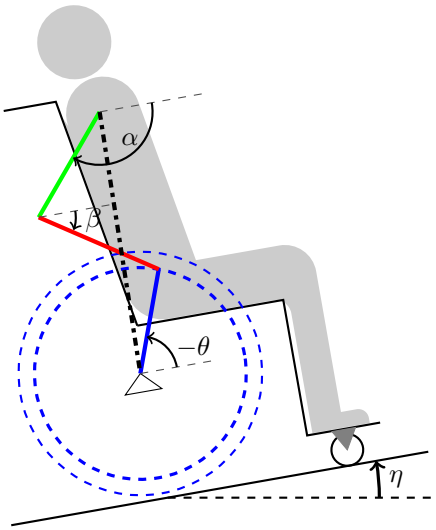

Figure 2. Moving four-bar system model to represent the wheelchair. The green line is the upper-arm, the red line is the lower-arm and the blue represents the pushrim of the wheelchair.

The model has three degrees of freedom (α, β, θ) in the recovery phase, and a single degree of freedom (θ) in the propulsion phase, where the contact between the hand and the pushrim is modeled as an ideal hinge joint. The dimensions and inertias of the mechanical system were estimated using anthropometric data for a person with 1.70 m of height and 70 kg of mass as reference (Winter, 2009), with rolling resistive force considered fixed as 20 N (Lenton *et al.*, 2008; van der Woude *et al.*, 2001). These parameters are listed in Tab. 1.

Table 1. Model parameters

Length Parameters		Mass Parameters	
User's height	1.7 m	User's mass	70 kg
Upper arms length (A)	0.3196 m	Upper arms mass (m_A)	3.9200 kg
Upper arms Center of Mass location (a)	0.2180 m	Upper arms Inertia (j_A)	0.0415 kg m^2
Forearms length (B)	0.2550 m	Forearms mass (m_B)	3.0800 kg
Forearms Center of Mass location (b)	0.1112 m	Forearms Inertia (j_B)	0.0439 kg m^2
Pushrim Radius (R)	0.2662 m	Rear Wheels Inertia (j_R)	0.2634 kg m^2
Rear wheel radius (R_r)	0.2988 m	Combined mass (body+wheelchair) (m_W)	72.5200 kg

Applying the Newton-Euler formalism, the equation of motion of the mechanical system for the recovery phase (Fig. 2)

in its minimal form can be written as:

$$\mathbf{M}(\mathbf{q})\ddot{\mathbf{q}} + \mathbf{k}(\mathbf{q}, \dot{\mathbf{q}}) = \mathbf{k_e}(\mathbf{q}) \tag{1}$$

where the generalized coordinates are:

$$\mathbf{q} = \begin{bmatrix} \alpha \\ \beta \\ \theta \end{bmatrix} \tag{2}$$

where $\mathbf{M}(\mathbf{q})$ is the mass matrix, $\mathbf{k}(\mathbf{q}, \dot{\mathbf{q}})$ is the vector of generalized Coriolis and centrifugal forces and $\mathbf{k_e}(\mathbf{q})$ is the vector of generalized forces.

In the contact phase, the angle between the upper arm and the horizontal plane (α) and the forearm and the horizontal plane (β) are dependent of the rear wheels angle (θ) via the two holonomic constraints:

$$\mathbf{c}(\alpha, \beta, \theta) = \begin{bmatrix} A\cos\alpha + B\cos\beta - R\cos\theta - h \\ A\sin\alpha + B\sin\beta - R\sin\theta - Y \end{bmatrix} = 0 \tag{3}$$

which form a hinge joint between the user's hand and the rear wheels of the wheelchair. h and Y are the horizontal and vertical distances between the shoulder and the center of the rear wheels of the wheelchair, respectively. The corresponding Jacobian matrix:

$$J(\alpha, \beta, \theta) = \frac{\partial q}{\partial \theta} \tag{4}$$

can be obtained from Eq. (3) and used to derive the single equation of motion for the propulsion phase from Eq. (1) as:

$$\mathbf{J}(\mathbf{q})^T\mathbf{M}(\mathbf{q})\mathbf{J}\ddot{\theta} + \mathbf{J}(\mathbf{q})^T\mathbf{M}(\mathbf{q})\frac{d\mathbf{J}}{dt}\dot{\theta} + \mathbf{J}^T\mathbf{k}(\mathbf{q}, \dot{\mathbf{q}}) = \mathbf{J}^T\mathbf{k_e}(\mathbf{q}) \tag{5}$$

where:

$$\dot{\mathbf{q}} = \mathbf{J}(\mathbf{q})\frac{d\theta}{dt} \tag{6}$$

The optimal control problem consists in searching for the system states and controls (joint moments) that minimize the cost function:

$$W = \frac{1}{t_f}\int_0^{t_f} (\tau_e^2 + \tau_s^2)\ dt \tag{7}$$

where τ_e and τ_s are the elbow and shoulder moments, respectively. This cost function quantifies the user effort along a complete propulsion cycle. For all the simulations, the wheelchair is considered in steady-state condition, i.e. the final states of the recovery phase ($t = t_f$) and the initial states of the propulsion phase ($t = 0$) are the same. The average locomotion speed was fixed by ensuring a constant ratio between the total displacement and the period along a complete cycle.

The simulations may converge to patterns where the contact angle span along the contact phase is small, which would lead to a higher push frequency and, consequently, higher chances of injuries (Rankin *et al.*, 2012). In order to avoid this tendency, the contact angle span over the pushrim is constrained to be larger than 50°, which is a lower-bound value found in experimental results found in the literature (Vegter *et al.*, 2014; Soltau *et al.*, 2015; Zukowski *et al.*, 2017). The final time t_f in the denominator of the cost function also favors longer cycle periods and, therefore, avoids the unwanted large push frequencies.

The elbow and shoulder moments (τ_e and τ_s respectively) where constrained to a peak of 80 Nm (40 Nm each side) to avoid unphysiological joint moments. This value is approximately the highest peak found in the literature for shoulder and elbow motions when propelling a wheelchair (39.7 Nm) (Sabick *et al.*, 2004).

The velocity was varied from 0.5 to 1.5 m/s with steps of 0.1 m/s. The slope angle was varied from 0° to 6° with steps of 1°. The optimal control problem was solved using a direct method based on the Radau Pseudospectral Method (Garg *et al.*, 2009) with the solver IPOPT (Wächter and Biegler, 2005). 100 collocation points were used for each state/control in each one of the 77 simulations, totalizing approximately 2000 variables per condition tested.

3. RESULTS

In Tab. 2 shows the classification of the simulated hand patterns for all the considered combinations of velocity and slope.

Table 2. Table of hand patterns predicted in the simulations: arcing over the handrim (AR), single loop above the handrim (SL), semi-circular pattern below the handrim (SC) and double-loop pattern (DL), see Fig. 1.

		Velocities [m/s]										
		0.5	0.6	0.7	0.8	0.9	1.0	1.1	1.2	1.3	1.4	1.5
Slope Angles [°]	0	SC	SC	SC	SC	DL	DL	DL	DL	DL	DL	DL
	1	SC	SC	AR	AR	DL	DL	DL	DL	DL	DL	DL
	2	AR	AR	AR	DL	DL	DL	DL	DL	DL	DL	DL
	3	DL	DL	DL	DL	DL	DL	DL	DL	DL	DL	DL
	4	DL	DL	DL	DL	DL	DL	DL	DL	DL	DL	DL
	5	DL	DL	SL	SL	SL	SL	DL	DL	DL	DL	DL
	6	SL	DL	SL	SL	SL	DL	DL	DL	DL	DL	DL

The results show the predominant occurrence of the semi-circular patterns under the handrim (SC) for lower speeds and slope angles. As slope and velocity increase, a consistent switch to the double-loop pattern (DL) is observed, going through the arcing over the handrim (AR) pattern. The SC pattern occurs mainly in lower slope angles (0° and 1°), as seen in Fig. 3, which shows the results for locomotion on an even surface at various speeds.

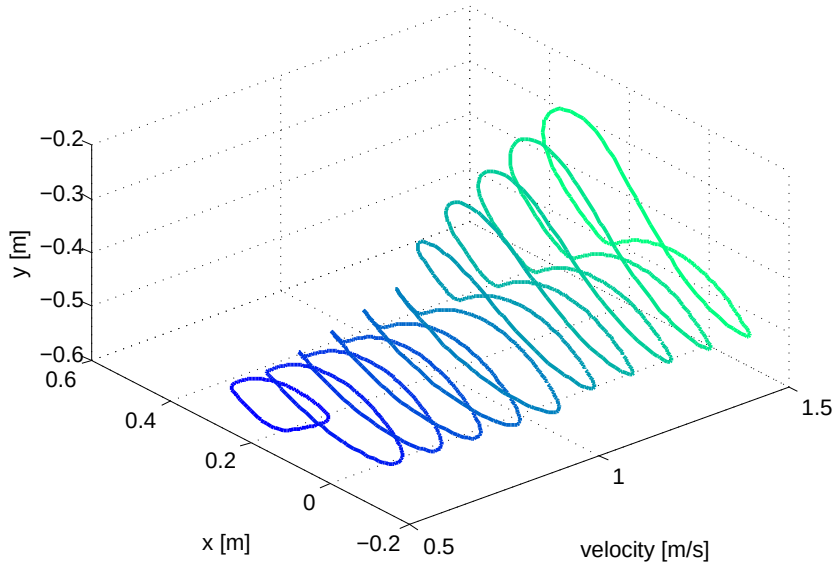

Figure 3. Predicted hand patterns at different velocities on an even surface.

Figure 3 shows a gradual transition from patterns below the hand-rim to the double-loop pattern. Except for the initial change (from velocity 0.5 to 0.6 m/s), substantial changes in the contact angle span could not be observed on an even surface, with maximal contact angles approaching the maximum achievable by the model with the parameters specified in Tab. 1.

With the increase of slope angle at some selected velocities, the hand trajectory went from an under the hand-rim pattern (SC) to a single-loop above the handrim pattern (SL), going through the double-loop pattern (DL), as clearly shown in Fig. 4.

Figure 4 shows that the hand pattern in the recovery phase gets gradually higher above the handrim with increasing slope angle, resulting finally in a single-loop pattern with a reduced contact angle span associated with a short recovery phase.

The contact angle span of the solutions with single-loop above the handrim pattern (SL) resulted in values close to 50°, which is the lower-bound constraint of this variable. The double-loop patterns, on the other hand, was consistently associated with larger contact angle spans.

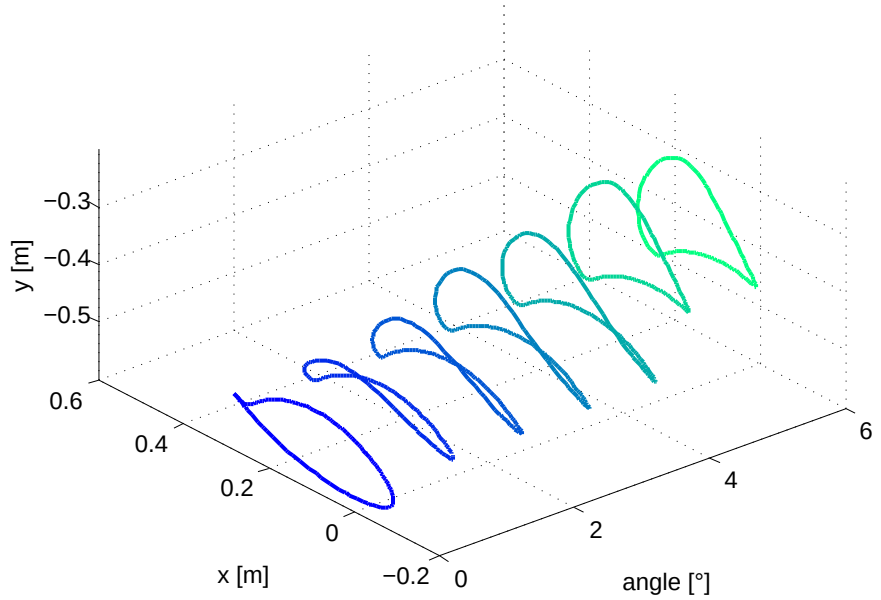

Figure 4. Predicted hand patterns at different slope angles for an average speed of 0.9 m/s.

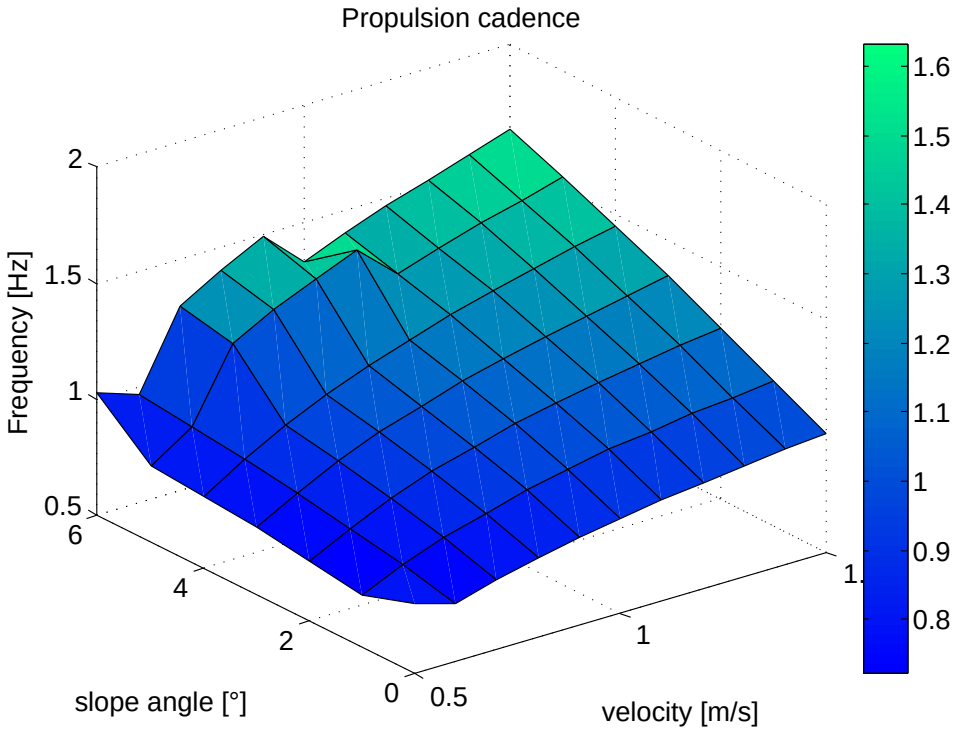

Figure 5. Predicted cadence of the wheelchair propulsion.

Figure 5 shows the predicted cadences of the wheelchair propulsion (cycles per second or Hz) for the different combinations of velocity and slope angle. The propulsion frequency gets higher with the increase of velocity and slope angle, going from the minimum of 0.8 Hz for locomotion on an even surface at 0.5 m/s to the maximum of 1.6 Hz for locomotion at 1.5 m/s with a slope angle of $6°$. The higher, dissonant region on the surface corresponds to the single-loop above the handrim patterns (SL) in Tab. 2, which are more compact patterns associated with shorter recovery phases and, therefore, larger propulsion frequencies.

Figure 6 shows the predicted cost function values for the combinations of mean velocity and slope angle.

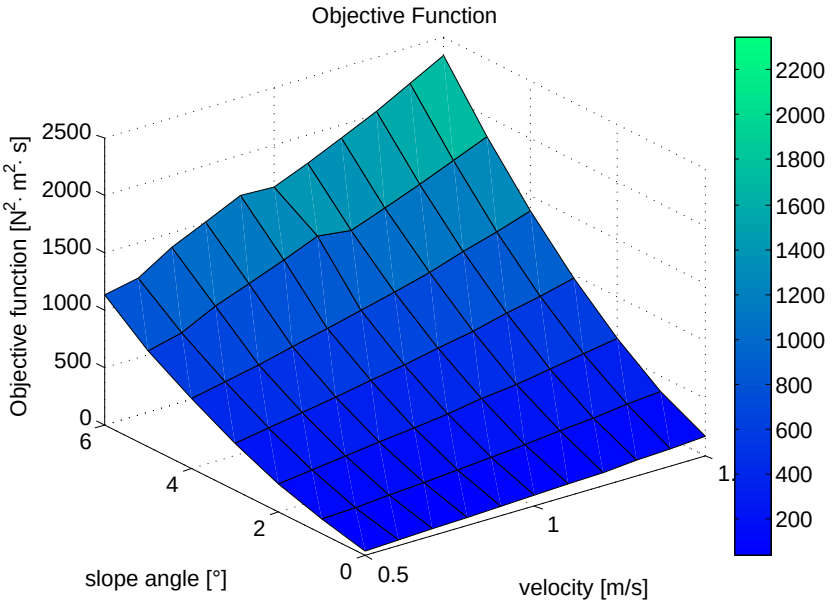

Figure 6. Predicted cost functions.

The cost function increases with slope angle and velocity, with slope angle having a larger impact than locomotion velocity. These results are consistent with the ones reported in Ackermann *et al.* (2014).

4. DISCUSSION

The propulsion technique affects the locomotion efficiency and the risk of injury in different ways. The double-loop pattern, predicted in the majority of conditions investigated in this study, has been related to lower cadence (push frequency) strategies (Boninger *et al.*, 2002), a beneficial effect because it reduces the cyclic demands on the upper extremity and also allows a longer recovery phase, reducing the overall muscle demand compared to other strategies (Slowik *et al.*, 2016). Experimental investigations also show the benefits of this pattern over the others (Kwarciak *et al.*, 2012).

The transition from trajectories under the rim to trajectories predominantly above the rim as velocity increases is consistent with data found in the literature (Slowik *et al.*, 2015). In lower velocities the arms tend to behave as a double pendulum under the effect of the gravitational field, justifying the trajectory below the pushrim. As inertial forces increase with velocity, the upper extremity starts undergoing a ballistic pattern, with the hand being projected forwards and upwards at the beginning of the recovery phase.

The faster recovery phase at increasing slope angles, related to the necessity of avoiding the wheelchair's backwards motion, favored a trajectory above the rim in our simulations. This is not consistent with data reported in the literature, which indicate patterns closer to the rim (Richter *et al.*, 2007). This is probably due to the fact that safety is not taken into account in the cost function in this study. It appears this is an important factor that leads to hand patterns closer to the rim on inclines.

Other possible source of this difference may be the forward lean of the user's trunk, which is more prominent in slopes than in level ground (Chow *et al.*, 2009). This lean could not be predicted by the model because the shoulder joint was admitted fixed in relation to the wheelchair as shown in Fig. 2. Besides the changes in the position of the center of mass, this lean can help the user propel in an angle closer to the horizontal plane ($\theta \rightarrow 0$, as shown in Fig. 2) which has better mechanical efficiency (Rozendaal *et al.*, 2003). Further studies may focus on implementing trunk and shoulder mobility in the model.

Regarding the single-loop above the handrim (SL) simulations specifically, the simulated contact angle span was substantially lower and the cadence larger than the ones observed in the other patterns (Fig. 5). In the literature, the single-loop pattern is reported as one of the most used patterns in wheelchair propulsion (Boninger *et al.*, 2002; Richter *et al.*, 2007), sometimes correlated mainly to inexperienced or non-trained wheelchair users (de Groot *et al.*, 2008). However, in recent studies, the SL is frequently considered more demanding than the double-loop and semi-circular patterns in terms of several biomechanical indicators, including muscle effort and risk of injury (Slowik *et al.*, 2016; Kwarciak *et al.*, 2012).

The higher cadence in the SL means that the user performs more cycles to cover the same distance compared to other patters such as the double-loop, increasing the risks of injury in the longer run.

The predicted wheelchair cadence (push frequency) is compatible with results reported in the literature, showing

similar dependency on velocity and slope angle (Chow *et al.*, 2009).

5. CONCLUSION

This study successfully applies an optimal control formulation to investigate the effects of wheelchair speed and slope angle on the hand trajectory over a complete propulsion cycle in steady-state conditions.

The increase in speed leads to a progressive transition from hand trajectories under the rim to hand trajectories above the rim with increasing influence of inertial forces, an observation consistent with findings in the literature. Increasing slope angles, in turn, was connected to progressively higher hand trajectories in the recovery phase, a pattern probably explained by the larger inertial forces associated with the decreasing duration of the recovery phase.

The presence of mainly semi-circular (SC) and double-loop patterns (DL) are in tune with the literature and consistent with their reported benefits compared to the single loop above the handrim (SL) pattern. The SL pattern appears scarcely, only for larger slope angle combinations, and is associated to a larger push frequency, increasing the risk of injury in the long run.

Further works based on this framework should incorporate the effects of cadence in the cost function and the mobility of the trunk and shoulder joint in the model.

6. REFERENCES

Ackermann, M., Leonardi, F., Costa, H.R. and Fleury, A.T., 2014. "Modeling and optimal control formulation for manual wheelchair locomotion: The influence of mass and slope on performance". In *5th IEEE RAS/EMBS International Conference on Biomedical Robotics and Biomechatronics*. IEEE.

Boninger, M.L., Souza, A.L., Cooper, R.A., Fitzgerald, S.G., Koontz, A.M. and Fay, B.T., 2002. "Propulsion patterns and pushrim biomechanics in manual wheelchair propulsion". *Archives of Physical Medicine and Rehabilitation*, Vol. 83, No. 5, pp. 718–723.

Chow, J.W., Millikan, T.A., Carlton, L.G., sik Chae, W., tae Lim, Y. and Morse, M.I., 2009. "Kinematic and electromyographic analysis of wheelchair propulsion on ramps of different slopes for young men with paraplegia". *Archives of Physical Medicine and Rehabilitation*, Vol. 90, No. 2, pp. 271–278.

de Groot, S., de Bruin, M., Noomen, S. and van der Woude, L., 2008. "Mechanical efficiency and propulsion technique after 7 weeks of low-intensity wheelchair training". *Clinical Biomechanics*, Vol. 23, No. 4, pp. 434 – 441. ISSN 0268-0033.

Garg, D., Patterson, M.A., Francolin, C., Darby, C.L., Huntington, G.T., Hager, W.W. and Rao, A.V., 2009. "Direct trajectory optimization and costate estimation of finite-horizon and infinite-horizon optimal control problems using a radau pseudospectral method". *Computational Optimization and Applications*, Vol. 49, No. 2, pp. 335–358.

Goosey-Tolfrey, V.L. and Kirk, J.H., 2003. "Effect of push frequency and strategy variations on economy and perceived exertion during wheelchair propulsion". *European Journal of Applied Physiology*, Vol. 90, No. 1-2, pp. 154–158.

Kwarciak, A.M., Turner, J.T., Guo, L. and Richter, W.M., 2012. "The effects of four different stroke patterns on manual wheelchair propulsion and upper limb muscle strain". *Disability and Rehabilitation: Assistive Technology*, Vol. 7, No. 6, pp. 459–463.

Lenton, J.P., Fowler, N.E., van der Woude, L. and Goosey-Tolfrey, V.L., 2008. "Wheelchair propulsion: effects of experience and push strategy on efficiency and perceived exertion". *Applied Physiology, Nutrition, and Metabolism*, Vol. 33, No. 5, pp. 870–879.

Rankin, J.W., Kwarciak, A.M., Richter, W.M. and Neptune, R.R., 2012. "The influence of wheelchair propulsion technique on upper extremity muscle demand: A simulation study". *Clinical Biomechanics*, Vol. 27, No. 9, pp. 879–886.

Richter, W.M., Rodriguez, R., Woods, K.R. and Axelson, P.W., 2007. "Stroke pattern and handrim biomechanics for level and uphill wheelchair propulsion at self-selected speeds". *Archives of Physical Medicine and Rehabilitation*, Vol. 88, No. 1, pp. 81–87.

Rozendaal, L., Veeger, H. and van der Woude, L., 2003. "The push force pattern in manual wheelchair propulsion as a balance between cost and effect". *Journal of Biomechanics*, Vol. 36, No. 2, pp. 239–247.

Sabick, M.B., Kotajarvi, B.R. and An, K.N., 2004. "A new method to quantify demand on the upper extremity during manual wheelchair propulsion". *Archives of Physical Medicine and Rehabilitation*, Vol. 85, No. 7, pp. 1151–1159.

Slowik, J.S., Requejo, P.S., Mulroy, S.J. and Neptune, R.R., 2015. "The influence of speed and grade on wheelchair propulsion hand pattern". *Clinical Biomechanics*, Vol. 30, No. 9, pp. 927–932.

Slowik, J.S., Requejo, P.S., Mulroy, S.J. and Neptune, R.R., 2016. "The influence of wheelchair propulsion hand pattern on upper extremity muscle power and stress". *Journal of Biomechanics*, Vol. 49, No. 9, pp. 1554–1561.

Soltau, S.L., Slowik, J.S., Requejo, P.S., Mulroy, S.J. and Neptune, R.R., 2015. "An investigation of bilateral symmetry during manual wheelchair propulsion". *Frontiers in Bioengineering and Biotechnology*, Vol. 3.

van der Woude, L., Veeger, H., Dallmeijer, A., Janssen, T. and Rozendaal, L., 2001. "Biomechanics and physiology in active manual wheelchair propulsion". *Medical Engineering & Physics*, Vol. 23, No. 10, pp. 713–733.

Vegter, R.J.K., de Groot, S., Lamoth, C.J., Veeger, D.H. and van der Woude, L.H.V., 2014. "Initial skill acquisition of handrim wheelchair propulsion: A new perspective". *IEEE Transactions on Neural Systems and Rehabilitation Engineering*, Vol. 22, No. 1, pp. 104–113.

Wächter, A. and Biegler, L.T., 2005. "On the implementation of an interior-point filter line-search algorithm for large-scale nonlinear programming". *Mathematical Programming*, Vol. 106, No. 1, pp. 25–57.

Winter, D.A., 2009. *Biomechanics and Motor Control of Human Movement*. John Wiley & Sons, Inc.

Zukowski, L.A., Hass, C.J., Shechtman, O., Christou, E.A. and Tillman, M.D., 2017. "The effect of wheelchair propulsion style on changes in time spent in extreme wrist orientations after a bout of fatiguing propulsion". *Ergonomics*, Vol. 60, No. 10, pp. 1425–1434.

7. RESPONSIBILITY NOTICE

The authors are the only responsible for the printed material included in this paper.